

PHYSICAL REVIEW FLUIDS **00**, 004200 (2017)**Drying regimes in homogeneous porous media from macro- to nanoscale**J. Thiery,^{1,2} S. Rodts,² D. A. Weitz,¹ and P. Coussot²¹*Experimental Soft Condensed Matter Group, School of Engineering and Applied Sciences, Harvard University, Cambridge, Massachusetts, USA*²*Université Paris-Est, Laboratoire Navier (ENPC-IFSTTAR-CNRS), Champs sur Marne, France*

(Received 10 February 2017; published xxxxxx)

Magnetic resonance imaging visualization down to nanometric liquid films in model porous media with pore sizes from micro- to nanometers enables one to fully characterize the physical mechanisms of drying. In larger pores, we identify an initial constant drying rate period, probing homogeneous desaturation, followed by a falling drying rate period. This second period is associated with the development of a gradient in saturation underneath the sample free surface that initiates the inward recession of the contact line. During this latter stage, the drying rate varies in accordance with vapor diffusion through the dry porous region, possibly affected by the Knudsen effect for small pore size. However, we show that for sufficiently small pore size and/or saturation the drying rate is increasingly reduced by the Kelvin effect. Subsequently, we demonstrate that this effect governs the kinetics of evaporation in nanopores as a homogeneous desaturation occurs. Eventually, under our experimental conditions, we show that the saturation unceasingly decreases in a homogeneous manner throughout the wet regions of the medium regardless of pore size or drying regime considered. This finding suggests the existence of continuous liquid flow towards the interface of higher evaporation, down to very low saturation or very small pore size. Paradoxically, even if this net flow is unidirectional and capillary driven, it corresponds to a series of diffused local capillary equilibrations over the full height of the sample, which might explain that a simple Darcy's law model does not predict the effect of scaling of the net flow rate on the pore size observed in our tests.

DOI: [10.1103/PhysRevFluids.00.004200](https://doi.org/10.1103/PhysRevFluids.00.004200)**I. INTRODUCTION**

Drying of micro- and nanoporous media is essential to a plethora of industrial processes such as the synthesis of drugs and cosmetics in the pharmaceutical sector, the treatment of soils in agriculture and oil recovery, and the use of concrete, plasters, and paints in the building industry. Although the understanding of this process is critical for minimizing energy consumption and controlling the final material properties, its scientific description is challenging as it involves a transient, spatially heterogeneous phase transition.

The basic phenomenological mechanisms of drying in simple systems initially filled with pure liquid have been identified [1–7]. After a short induction period of variable duration, a constant drying rate period (CRP), associated with a homogeneous desaturation of the medium, usually occurs. In particular, in this regime capillary equilibration processes allow for water redistribution throughout the whole medium [1,8–11]; since the vapor density conditions are approximately conserved around the surface of evaporation of the sample the apparent constant drying rate is preserved. This regime is followed by a falling drying rate period (FRP) and more or less simultaneously the appearance of a heterogeneous saturation profile [1,8–11]. There is a critical interest in this transition in practice as it reveals tendencies to water retention and shows a possible dramatic decrease of the drying rate. The exact conditions for this FRP to start as well as the evolution of the liquid distribution within the medium in this regime are not yet well determined and understood, except in the case of gravity dominated flow, with a focus on soils [12–16]. It is generally considered that the onset of this second regime results from a demand of liquid, through the imposed evaporation rate, larger than the liquid flux towards the free surface and resulting from capillary effects. Such a situation would lead the

J. THIERY, S. RODTS, D. A. WEITZ, AND P. COUSSOT

inward growth of a dry region from the sample free surface [1,4,7]. In detail, it was also suggested that two FRPs should be considered [4,17–19], associated with the continuous and the discontinuous states of the liquid network. The development of a receding dry front was observed and measured in a variety of cases, such as experiments with a nonwetting liquid [20], accumulation of ions [21] or particles [22,23] below the free surface, a packing filled with a paste [10], and a packing of large beads [23], and in all cases the drying rate in this second regime was probed to scale as the diffusion of vapor from the wet front to the free surface. However, due to the limited possibilities of internal observations, up to now we have ignored what determines this transition, what are the processes of liquid flow in that period, and what is the impact of the porous media characteristics (e.g., pore size) on these phenomena.

In this work, we use a magnetic resonance imaging (MRI) profiling technics to gain access to the liquid distribution in time within model porous media with pore size covering almost four decades down to the nanometer scale. This measurement enables one to characterize the physical processes governing drying in the FRP regime and in particular to investigate the dynamics of liquid and vapor transport in these model systems.

This paper is organized as follows. In Sec. II we describe the materials synthesized and the measurement tool used. Section III aims at presenting a discussion of our results and models; eventually, our conclusion is featured in Sec. IV.

II. MATERIALS AND METHODS

A. Materials

We focus on the simplest model porous media, i.e., bead packings, in the form of particulate gels with a solid volume fraction (i.e., $\phi_0 = 58 \pm 3\%$) approaching the maximum (disordered) value. These gels are made of amorphous aggregated and almost monodispersed silica particles of diameter $2R = 6, 12, \text{ and } 40 \text{ nm}$ (Ludox SM-30, HS-40, and TM-40, respectively, provided by Sigma-Aldrich) or of diameter $2R = 80, 300, 1000, \text{ and } 1500 \text{ nm}$ (provided by Fiber Optics Center), suspended in water. The deviation from nominal size was measured to 6% on average. Also, we manufactured a sample with $2R = 45 \mu\text{m}$ glass beads by pressing and heat-sintering beads together. Note that silica and glass both have hygroscopic surfaces.

For bead diameters of 40 nm and smaller the samples are initially prepared as gels with a solid fraction of 20%. These gels are further dried on a nonadhering substrate, allowing them to shrink in a homogeneous manner under the action of capillary forces [24]. During shrinkage the gels remain saturated [24,25]; however, when shrinkage stops, the sample starts to desaturate—this regime constitutes the stage of interest within the present frame. Using MRI, we previously demonstrated our ability to distinguish between the saturated and nonsaturated regimes during this process [25]. Here we show only the saturation profiles starting from the last saturated profile recorded, i.e., just at the end of the homogeneous shrinkage. At that time, we observed that the sample concentration was around 58%.

Samples made with a bead diameter of 80 nm and larger are formulated by dispersing anhydrous particles in water. These suspensions are then centrifuged (5000 rpm for 35 min) so as to form a continuous network of particles in contact and to remove most bubbles. This granular paste is then placed in the Petri dish and gelled with the same protocol as above.

Concerning gel synthesis, in the initial state, aggregation of particles is initiated by the addition of NaCl to a concentration of 0.5 mol l^{-1} (for bead diameters smaller than 80 nm) or MgCl_2 to a concentration of 0.025 mol l^{-1} (for bead diameters equal to or larger than 80 nm), which ensures complete gelation after several days. This process simultaneously brings interparticle cohesion by means of liquid phase sintering [26].

Once the samples are gelled, for the smallest beads, 97% of the salt initially incorporated is removed from the system through a special dialysis protocol [25]. The amount of NaCl extracted after each dialysis was evaluated by performing conductivity measurements on dialysates. The

DRYING REGIMES IN HOMOGENEOUS POROUS MEDIA . . .

98 remaining concentration of salt within the gels prior drying is about 1 g l^{-1} , which ensures, since the
 99 solubility of NaCl at 20°C is 360 g l^{-1} , that no crystallization occurs below a saturation of the order
 100 of 0.003. For the largest beads no dialysis is carried out and the concentration of salt within the gels
 101 prior drying is about 2.4 g l^{-1} , which ensures, since the solubility of MgCl_2 at 20°C is 542 g l^{-1} , that
 102 no crystallization starts before a saturation of 0.004 is reached. Moreover, since the Péclet number
 103 [defined as VH/D , where V is the drying velocity (see definition below), H the sample thickness,
 104 and D the diffusion coefficient of salt in water] is smaller than 0.1, salt advection can be considered
 105 negligible. Finally, since such very low (average) saturations are reached only for the largest beads
 106 in the very last stages of drying (see Fig. 1), i.e., when the drying front is close to the sample bottom,
 107 we conclude that crystallization will possibly occur in these very last stages, and in a homogenous
 108 way throughout the remaining wet region.

109 After the gelation procedure all our samples were sufficiently rigid to be handled without breaking.
 110 The samples with the largest beads were the weakest. At the end of drying, the samples were in
 111 a similar state (i.e., rigid). We conclude that the granular material is consolidated; i.e., no relative
 112 motion of the particles is expected during the drying process.

113 Due to the preparation procedure, the samples were *a priori* saturated initially. Visual observation
 114 of the fully wet free surface of the sample tends to confirm this statement. The curvature of the
 115 initial MRI saturation profiles sometimes observed at the approach of the sample top (see Fig. 1) is
 116 not an artifact of the technique. This is essentially due to the initial nonplanar shape of the sample:
 117 a meniscus along the peripheral edge and some concavity of the free surface towards the center. On
 118 the other hand, the curvature of the profiles at the sample bottom is due to the fact that the Petri
 119 dishes were not flat.

120 The samples were then put to dry inside the MRI magnet. Due to this specific protocol of
 121 concentration from a flocculated structure, which might be initially fractal [27], these packings may
 122 not be perfectly homogeneous at some scale; e.g., there may remain some larger pores distributed
 123 throughout the sample. However, considering the high average volume fraction, the majority of pores
 124 must correspond to that expected for a disordered bead packing. Consequently, if such heterogeneities
 125 happen to play a role during drying this could only be over a very narrow range of saturations just
 126 below 1; in any other situation the drying characteristics rely on the extraction of liquid from the rest
 127 of the sample, which can be considered a packing with homogeneous pore size distribution scaling
 128 with the particle diameter. Under these conditions the strong interest of these materials is that,
 129 *a priori*, since their porous structure remains similar while only one characteristic length scale (i.e.,
 130 particle size) varies, we can rely on them to allow us to probe the sole effect of pore size on the
 131 drying characteristics when it varies from a couple of microns to a few nanometers.

132 **B. Setup**

133 Initially the cylindrical samples are saturated with water; therefore, the solid matrix is completely
 134 wet, and only the top surface is open to air. We induce a constant dry air flux (adsorption drying,
 135 relative humidity below 0.5%) vertically against the sample free surface at a given flow rate (0.3 m/s),
 136 and we follow the drying thanks to NMR measurements (see below). The samples are prepared in
 137 Petri dishes of inner diameter 9.6 cm. In some cases the thickness of the material was slightly smaller
 138 (by a couple of millimeters) than the height of the dish edge, but this does not significantly affect
 139 the drying process or our analysis of the data for the following reasons: the air flux is vertical, which
 140 ensures that all the sample surface is reached by this flux; the level difference between the free
 141 surface and the top edge of the dish is much smaller than the sample diameter, so the perturbation
 142 on the flow is limited to a negligible region at the sample periphery; and for a given sample this
 143 potential slight perturbation affects the drying rate in the same way at any time, so our analysis based
 144 on a rescaling of the current drying rate by the initial one *a priori* removes the possible impact of
 145 this effect.

146 The sample thickness (H) is in the range 5–10 mm, except for the $45\text{-}\mu\text{m}$ -diam beads (25 mm).
 147 Under such conditions the characteristic stress due to gravity ($\rho g H$, with ρ the water density and g

J. THIERY, S. RODTS, D. A. WEITZ, AND P. COUSSOT

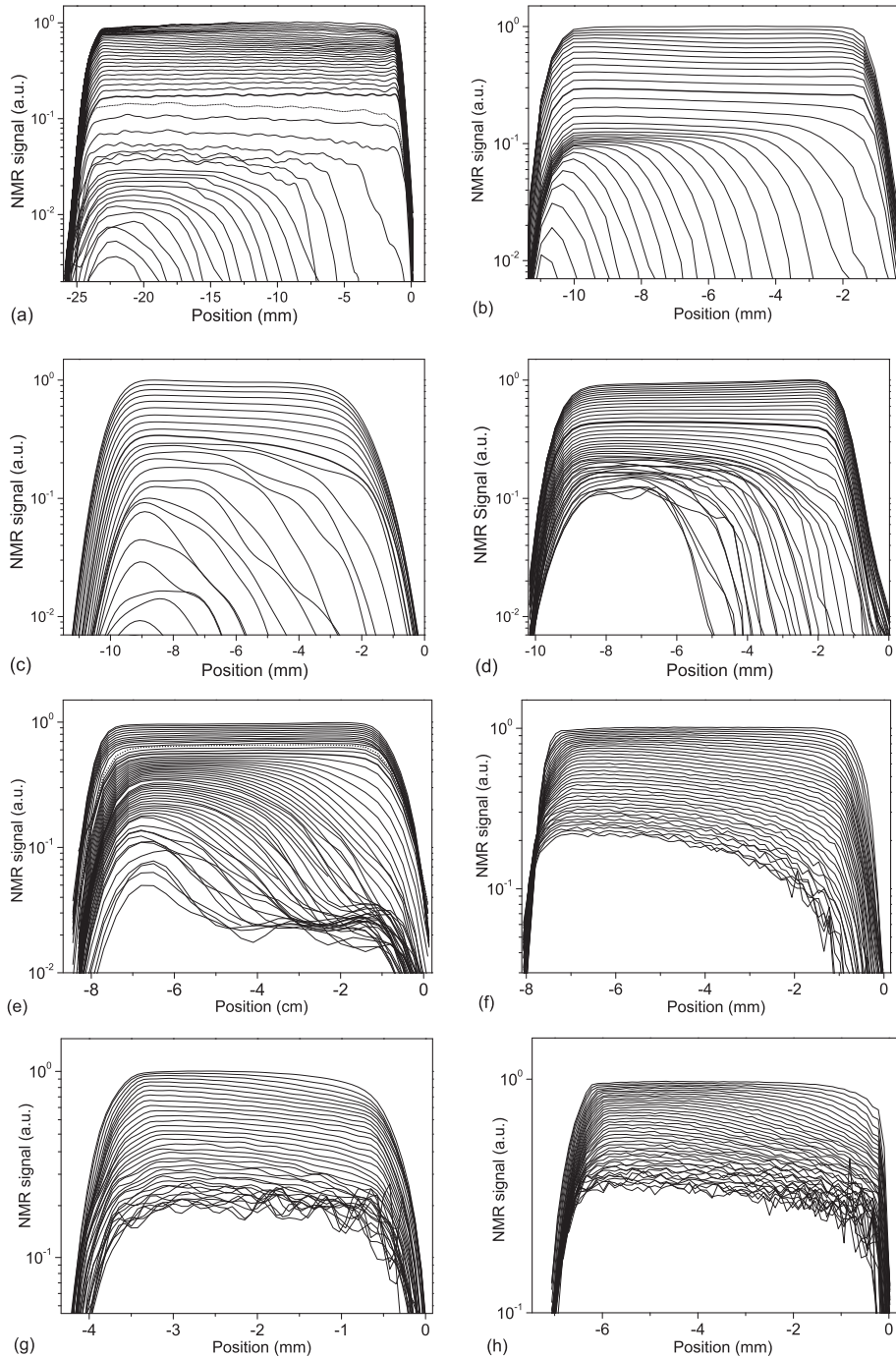


FIG. 1. NMR profiles along sample axis at different times (time interval Δt) (from top to bottom) during drying for bead packings with different particle diameters: (a) 45 000 nm (time interval of 23, then 44 min), (b) 1500 nm (33 min), (c) 1000 nm (36 min), (d) 300 nm (50 min), (e) 80 nm (33 then 44 min), (f) 40 nm (28 min), (g) 12 nm (16 min), and (h) 6 nm (23 min). The first profile with some gradient in saturation is represented by a thicker line. The dotted line corresponds to the first profile after the time interval change. Note that for the sake of clarity data for 300 and 80 nm in the FRP have been smoothened.

DRYING REGIMES IN HOMOGENEOUS POROUS MEDIA . . .

148 the gravity) is smaller than 200 Pa, while the characteristic capillary stress (σ/r , with σ the surface
 149 tension and r a typical pore size, say, $r \approx R/3$) is larger than 10 000 Pa. This means that gravity
 150 effects are fully negligible in all our tests.

151 The drying velocity (or drying rate, V) is defined as the equivalent liquid volume crossing the
 152 sample free surface cross section per unit time and surface. We thus have $V = -\varepsilon H d\bar{\psi}/dt$, in
 153 which $\bar{\psi}$ is the average saturation (ratio of water to pore volume) in the sample and ε the sample
 154 porosity ($\varepsilon = 1 - \phi_0$). In order to determine this velocity we rely on NMR measurements (water
 155 content profiles in time) that are taken with relatively large time intervals. This explains that we
 156 cannot precisely observe the fast decrease in drying rate in the very first times of drying of a porous
 157 medium occurring as a result of the evaporation of some liquid layer covering the sample free surface
 158 and until the formation of the first liquid meniscus in this region. In the next step, which roughly
 159 corresponds to what we could effectively observe from our measurements, the drying rate depends
 160 on the interaction between the air flux and the specific shape of the liquid-air interface at the sample
 161 free surface, which may depend on the porous medium characteristics. It appears that our imposed air
 162 flux induces different initial drying velocities (V_0), decreasing from 0.052 to $0.02 \pm 0.004 \text{ cm h}^{-1}$
 163 for bead sizes from 45 microns to 6 nm.

164 Note that previous works showed that the impact of increasing external flux, in terms of the
 165 duration of the CRP before reaching the FRP, is qualitatively equivalent to reducing pore size [4].
 166 This means that even if we do not here proceed to systematic tests at different values of external
 167 fluxes we can infer that the trends observed when decreasing the pore sizes would be qualitatively
 168 similar if the external flux velocity was increased, but the exact variations constitute a field to explore.
 169 Moreover, the above statement is *a priori* not valid if the Kelvin effect starts to play a significant
 170 role (see below), i.e., for sufficiently small pores and/or saturation.

171 **C. MRI measurements**

172 The distribution of apparent water along the sample vertical axis (z) is measured by placing the
 173 sample at the magnetic center of the gradient coil of a 24/80 DBX 0.5-T ^1H MRI spectrometer by
 174 Bruker (20 cm open diameter in the sample area) and running a one-dimensional double spin-echo
 175 measurement (two first echoes of the so-called CPMG sequence [25]). An exponential extrapolation
 176 was verified and used to compensate for spin-spin relaxation [28]; specifically, the unbiased proton
 177 density [$\rho_0(z)$, directly relating to the water content] was extrapolated as $\rho_0(z) = \rho_1(z)^2/\rho_2(z)$, where
 178 $\rho_1(z)$ and $\rho_2(z)$ are the signal proton density owing to the first and second echoes, respectively.
 179 Although established under the hypothesis of monoexponential relaxation, this type of extrapolation
 180 can still be shown to provide a reliable estimate of the amount of water present even in slight
 181 multiexponential cases, provided echo times are set short regarding the shortest relaxation time in
 182 the sample (in the case of very low sample saturation). Therefore, each measured value of this
 183 distribution corresponds to the total amount of water in a thin cross-section layer varying from 75
 184 to 500 μm thickness along the vertical axis of the Petri dish depending on chosen space resolution;
 185 we yield the distribution of water in small cross-section layers along the sample axis at different
 186 positions and time. Note that the maximum reachable resolution is limited by both sample-induced
 187 inhomogeneities of the magnetic field in the MRI magnet and the intrinsic relaxation properties of
 188 each sample and therefore may vary from one sample to the other (see [29]).

189 Eventually, at extremely low proton density the limitation of the dual echo measurement is
 190 inevitably reached, which triggers the need to smooth the profiles measured to enhance interpretation
 191 of their shape. The smoothing filter we apply corresponds to convolution by means of a Gaussian
 192 distribution $g(z) = \exp(-z^2/2\sigma^2)$, with a full width at half maximum σ empirically set to 2.3–
 193 4.1 pixels. Since the amplitude of measured profiles may suffer some baseline overestimation at very
 194 low signal, this filter is applied to the complex profiles of each echo before its amplitude is treated
 195 and prior to extrapolation. Note that when this filter is applied, the resolution of the profile can be
 196 considered blurred and the new pixel size increases roughly by a factor of 3.5–6. Data of the order
 197 of the noise level were removed.

J. THIERY, S. RODTS, D. A. WEITZ, AND P. COUSSOT

198 Note that at the end of their preparation, due to the meniscus effect and the container shape, the
199 sample top and bottom are slightly curved, which induces the appearance of ramps on the profiles,
200 i.e., a progressive decrease of the NMR signal over the millimeter order even if the saturation in
201 the sample is homogeneous (see Fig. 1). The local saturation (ψ) may be obtained by dividing the
202 current local NMR signal by the initial one at the same point (when it exists), but a representation
203 of the NMR signal provides clearer information on the saturation evolution around the top and the
204 bottom of the sample.

205 III. RESULTS AND DISCUSSION

206 A. Saturation profiles during drying

207 The saturation profiles (represented in terms of extrapolated NMR signal, for the reasons explained
208 above) at different times during drying of each sample are shown in Fig. 1. In these figures the first
209 (upper) profile corresponds to a saturated sample and the next ones to a partially saturated sample,
210 with a saturation corresponding to the current ratio of the NMR signal value to the initial value at
211 the same position in the sample. Note that in some cases we adjusted the NMR sequence parameters
212 during the drying, without pausing the experiment, to optimize the resolution and reduce the noise
213 level; this could be performed a couple of times during the same experiment and explains some
214 variations in the aspect (spacing, smoothness) of the series of profiles with time. The reproducibility
215 of these data has been verified by repeating several of these tests up to three times. Some slight
216 differences could be observed in the exact evolution of the shape of the profiles, especially at low
217 saturation, but within the frame of our analysis this is negligible. Our representation of these profiles
218 in logarithmic scale is allowed thanks to the good signal to noise ratio of our data, which thus
219 provides information concerning the distribution of liquid water in the samples down to a saturation
220 of 0.1% for the beads larger than 1 micron. Obviously, the smallest saturation observed increases as
221 the beads become smaller, since the thickness of the liquid films reaches the molecular size at larger
222 saturation (we analyze this point further below).

223 For bead sizes down to 80 nm we observe a first period during which, while decreasing, the
224 saturation remains almost perfectly homogeneous: in a logarithmic scale the profiles remain strictly
225 parallel [see Figs. 1(a)–1(e)]. This means that although water is withdrawn in the form of vapor from
226 the top surface of the sample a balance of capillary effects is maintained throughout the sample
227 whatever the value of the average saturation in this regime. Thus, as air enters the sample, there
228 is a liquid “counterflow” directed towards the sample free surface which makes it possible to keep
229 a uniform (Laplace) pressure throughout the sample, an effect already identified in the literature
230 [4,30,31]. However, as a result of the increasing withdrawal of liquid in the top layers of the sample,
231 this liquid motion occurs in the form of successive bursts of capillary reequilibration throughout the
232 complex disordered medium [16,32,33]. A recent pore network modeling, which proved to be able
233 to well predict the CRP characteristics and the occurrence of the second stage, provides a further
234 view of the physical effects at a local scale [34]. Note that it was also proved from simple mass
235 conservation arguments that, if the saturation decreases homogeneously in time, the liquid velocity
236 increases linearly from the bottom to the top of the sample [34].

237 Within some uncertainty on the exact moment of its onset (i.e., first homogeneous partially
238 saturated state), and even if, sometimes, significant fluctuations are observed during that period,
239 this regime is essentially associated with a constant drying rate. This so because (i) At a very
240 short distance from the first liquid-air interface the vapor density is at its maximum and likewise in
241 depth, as the air pockets are surrounded by liquid-air interfaces; consequently, evaporation mainly
242 occurs from the first liquid-air interface (around the sample free surface) where a significant vapor
243 density gradient is expected [35]. (ii) The liquid transport towards the free surface maintains a set of
244 liquid-air interfaces (liquid patches) in that region, which in turn can maintain a (constant) maximum
245 vapor density around almost the same position below the air flux so that the boundary conditions for
246 evaporation remain constant [36,37].

DRYING REGIMES IN HOMOGENEOUS POROUS MEDIA . . .

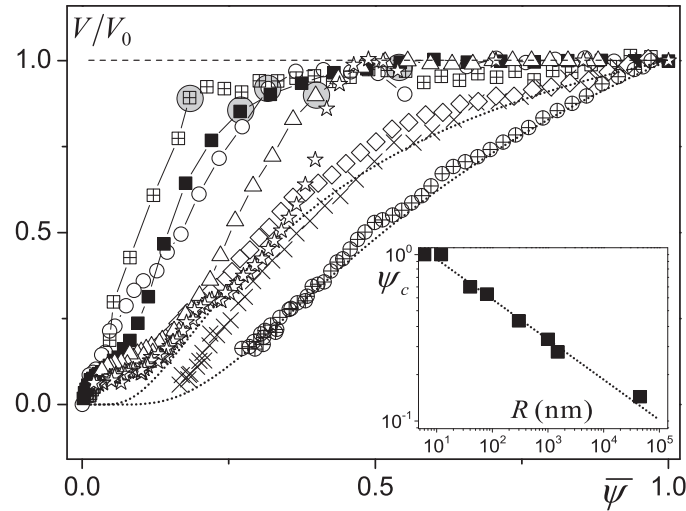


FIG. 2. Drying velocity (rescaled by the initial one) as a function of the saturation for bead packings with different bead diameters: 45 000 nm (cross squares), 1500 nm (solid squares), 1000 nm (circles), 300 nm (triangles), 80 nm (stars), 40 nm (diamonds), 20 nm (crosses), 6 nm (cross circles). The position of the first MRI profile (see Fig. 1) with saturation gradient is shown with a grey disk. The dotted lines correspond to the model based on the Kelvin effect (see text). The inset shows the critical saturation, associated with the formation of a gradient in the saturation profile, as a function of the particle radius. The dotted line in the inset corresponds to $\psi_c = 1.8R^{-1/4}$, with R in nanometers.

247 Below some critical saturation (ψ_c), a saturation gradient appears below the sample free surface
 248 (see Fig. 1); i.e., the corresponding saturation profile is no longer parallel to the previous one. Around
 249 the same time the drying rate starts to decrease (see the grey disks in Fig. 2). This occurs sooner
 250 (i.e., for larger ψ_c) for smaller bead radius.

251 For the largest beads (≥ 40 nm), we can then observe the development of a region, just below the
 252 free surface, where the saturation profiles drop to very small values [not larger than the noise; see
 253 Figs. 1(a)–1(d)]. This may be considered an apparent dry region, i.e., one from which no more liquid
 254 can be extracted, and we measure the thickness of this region (h) from the NMR saturation profiles.
 255 Note, however, that this apparent dry region in fact corresponds to a region where no NMR signal
 256 larger than the noise could be detected. The corresponding critical liquid content, i.e., that below
 257 which no relevant signal can be measured, depends on the sample relaxation characteristics along
 258 with our NMR parameters chosen; however, measurement of the dry mass of the samples (after 24 h
 259 spent in the oven postdrying) confirmed a negligible residual amount of water. The strong drop in
 260 saturation observed in logarithmic scale around some positions in our profiles (see Fig. 1) anyway
 261 suggests that if there remains some liquid in the apparent dry region its thickness is very small, of
 262 the order of the molecular size. It happened that for the 80-nm beads the NMR parameters allowed
 263 us to also get relevant measurements in this region [see Fig. 1(e)]: there we see an apparent uniform
 264 level from the front of the dry region to the free surface of the sample. In order to estimate the typical
 265 thickness (e) of the liquid films let us assume that the liquid present in the porous medium is equally
 266 distributed at the surface of the beads. In that case, we have $4\pi e R^2 / (4\pi R^3 / 3) = (1 - \phi_0)\psi / \phi_0$, so
 267 that $e \approx 0.24R\psi$. We find a plateau at a saturation around 3%, which corresponds to an average
 268 liquid film thickness of 0.29 nm, of the order of the water molecule diameter (0.34 nm).

269 This suggests that there remains a molecular thick layer adsorbed on the solid surface, even in a
 270 region usually assumed to be dry, in the ultimate stages of sample drying under convection, possibly
 271 resulting from an adsorption equilibrium with the residual water contained in the “dry air” flow.
 272 This is confirmed by the data for smaller bead sizes [see Figs. 1(f)–1(h)]. Here the profiles appear

J. THIERY, S. RODTS, D. A. WEITZ, AND P. COUSSOT

273 to become very noisy and almost stagnant, below a saturation around the critical value for which,
 274 according to the above formula, the liquid film thickness is of the order of the molecule size. As the
 275 next profiles were greatly affected by the measurement noise, we skipped their representation. This
 276 rapid development of the noise in fact suggests that the number of mobile liquid water molecules
 277 tends to zero, except for a thin layer of poorly mobile adsorbed water molecules on the solid surface.

278 For the 40-nm-diam beads a dry front starts to develop from the very beginning of drying [see
 279 Fig. 1(f)], apparently in the continuity of the observations for larger beads. However, the drying
 280 front eventually does not spread very deep and its position seems to reach an asymptotic value
 281 while the rest of the sample desaturates almost homogeneously. For smaller beads no more dry front
 282 appears; the sample immediately desaturates almost homogeneously [see Figs. 1(g) and 1(h)]. Thus
 283 it appears that the drying characteristics of nanoporous materials exhibit specific trends. This is not
 284 so surprising as we are here dealing with materials with a pore size of the order of a few molecules.
 285 For example, for the 12-nm beads, the typical pore size is 2 nm, which is six times the molecule size.
 286 In that case, the concept of thermodynamic phase is not relevant, so one cannot expect that some
 287 liquid could simply drain towards the sample free surface as a result of standard capillary effects
 288 [38]. It is remarkable that for nanopores there is apparently an effect playing a similar role, thus
 289 allowing homogeneous desaturation of the sample during drying.

290 B. Drying rate

291 Let us attempt to quantify the evolution of the drying rate according to these observations. Just
 292 before the transition between CRP and FRP the relative humidity n is equal to 1 at the sample free
 293 surface and drying may be described as vapor diffusion, from the air-liquid interface, through a
 294 boundary layer (of air) of thickness δ , and up to a region where $n = 0$. Under such conditions, from
 295 the Fick's second law, we obtain $V_0 = (\rho_0/\rho)D_0/\delta$, with $D_0 = 2.7 \times 10^{-5} \text{ m}^2 \text{ s}^{-1}$ the water vapor
 296 diffusion coefficient in air, and $\rho_0 = 23.4 \text{ g m}^{-3}$ the maximum vapor density in air (at 25 °C). Later
 297 on, when a dry region has developed inside the sample from its free surface, we can still assume for
 298 the sake of simplicity that the liquid evaporates exactly from the limit of the wet region (where $n = 1$)
 299 and the vapor diffuses to the free surface over a distance h , i.e., the thickness of the dry region, before
 300 reaching the external boundary layer. Now the relative humidity at the sample free surface is n_1 and
 301 the drying velocity is $V = n_1 \rho_0 D_0 / \rho \delta = n_1 V_0$. In addition, the vapor density gradient along the dry
 302 region induces a vapor flux which can be expressed in steady state as $V = \rho_0 D_v (1 - n_1) / \rho h$, where
 303 D_v is the vapor diffusion coefficient through the (dry) porous medium. We can write D_v as $\varepsilon D_0 / \tau$,
 304 where τ the tortuosity of the medium [30]. Note that in this description D_v appears independent
 305 of the bead size, which translates into the assumption of the kinetics of vapor diffusion not being
 306 affected by pore size.

307 From the two above expressions for the vapor flux we deduce $n_1 = 1/(1 + D_0 h / D_v \delta)$, and the
 308 drying rate can be written as $V = \rho_0 D_v / \rho (h + \delta^*)$ with $\delta^* = D_v \delta / D_0$. This may be rewritten as

$$[(V_0/V) - 1] = (\rho/\rho_0 D_v) h V_0. \quad (1)$$

309 Let us compare this theoretical prediction with our data. In this frame the most difficult point is
 310 the determination of h . Since in logarithmic scale the saturation profiles exhibit a vertical asymptote
 311 at some distance from the sample top, it is natural to consider this distance as the thickness of the dry
 312 front. However, in such profiles, we ignore if the saturation gradient, which progressively extends
 313 over a longer distance as the dry front progresses, is due to a homogeneous variation of the saturation
 314 in the sample or to some heterogeneity of the advancing front structure. Finally, we ignore if the
 315 position at which we should consider that $n = 1$ is situated at the vertical asymptote or at some
 316 distance behind, within the saturation gradient. For the calculations here, we keep the first option.

317 For $R \geq 40 \text{ nm}$ we observe a first stage during which the data plotted in terms of $[(V_0/V) - 1]$
 318 vs $h V_0$ effectively follow a master curve of slope 1, in a larger range of dry region thickness when
 319 the bead radius increases (see Fig. 3); this period lasts for up to two decades of dry front thickness
 320 for the largest beads, in agreement with the prediction of Eq. (1). Therefore, our measurement of

DRYING REGIMES IN HOMOGENEOUS POROUS MEDIA ...

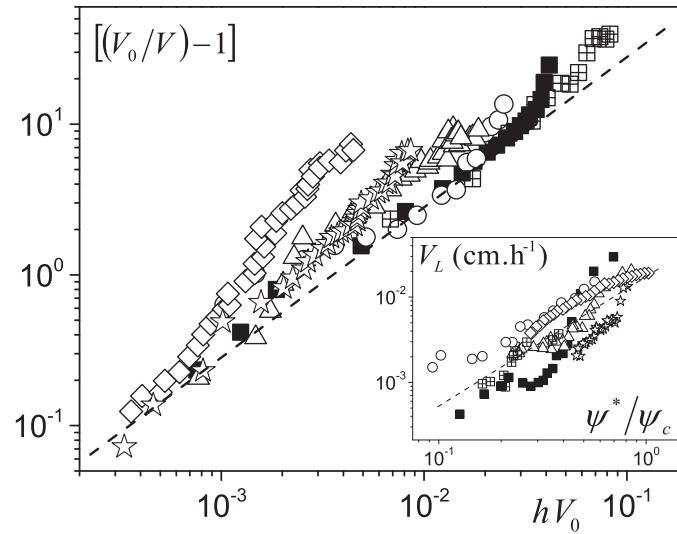


FIG. 3. Evolution of a function of the rescaled velocity (which may also be seen as the deviation from the drying rate in the CRP) as a function of the thickness of the dry front times the initial velocity for the different bead sizes (same symbols as in Fig. 2). Dotted line has a slope of 1. The inset shows the mean liquid velocity in the wet region as a function of the mean saturation in this region.

321 the height of the dry region from the position of the NMR profile appears consistent, as well as the
 322 assumption of a unique diffusion coefficient through these similar porous media down to slightly
 323 more than diameters of 300 nm. In this regime, the value for D_v extracted from the straight line
 324 fitted to this master curve corresponds to a tortuosity $\tau = 2.5 \pm 0.2$, which is significantly larger
 325 than the ratio of the length of the effective path of a molecule to skirt the grain to its diameter, i.e.,
 326 $\pi/2 \approx 1.6$. This suggests that the effective position for which $n = 1$ is in fact situated at some slight
 327 distance behind, in the region of saturation gradient, by a more or less constant factor (say, between
 328 1.2 and 1.5) which would shift the data of Fig. 3 to the right, leading to a larger diffusion coefficient
 329 and a smaller tortuosity.

330 Despite this difficulty, the variations are as expected from the theory, so these results confirm the
 331 consistency of a description of drying in porous media in a wide range of pore sizes in two stages:
 332 a CRP followed by a FRP during which a dry front recedes and the drying rate results from vapor
 333 diffusion from the dry front. Additionally, this analysis shows that even if there may remain some
 334 adsorbed liquid layer on the beads in this dry region, not detected by our NMR measurements, it
 335 does not play a significant role in drying process.

336 From 300 nm and smaller diameters we observe a progressively larger deviation of the data from
 337 the master curve, constituting a second stage in the evolution of the apparent
 338 dry region. Since the physical scheme of regime 1 appeared valid at larger diameters it is natural to
 339 consider that some specific effect due to the small pore size could play a more and more important
 340 role as the diameter decreases. In this context, one may think of an impact of the Knudsen effect for
 341 bead diameter less than $1 \mu\text{m}$ since in this case the pore size is not much larger than the mean free
 342 path of the water molecules (i.e., $l \approx 80 \text{ nm}$ under a pressure of 1 atm), which is known to affect the
 343 coefficient of diffusion. As a first approximation, we can describe this effect over the whole range
 344 of pore sizes by considering that the diffusion coefficient is in fact $D = \xi D_v$, with $\xi = (1 + l/L)^{-1}$
 345 [39]. This shows that this effect should tend to shift the data as a whole above the theoretical curve
 346 (i.e., towards lower values of hV_0) in Fig. 3, by a factor depending on the bead size but independent
 347 of other characteristics (dry region thickness, saturation, etc). We ignore the exact value of L for
 348 a porous medium (for a straight channel this is the channel diameter) but if it was of the order of

J. THIERY, S. RODTS, D. A. WEITZ, AND P. COUSSOT

349 the typical pore size the coefficient ξ would be significantly smaller than 1 for $R \leq 300$ nm. This
 350 is not what we observe: the data first follow a curve of slope 1, approximately independent of R ,
 351 for small h values, then they start to depart from this curve by a coefficient increasing with h (see
 352 Fig. 3). Finally, there is a clear departure from a straight line of slope 1 for small R , as clearly
 353 appears for $R = 40$ and $R = 80$ nm. Thus, it seems like the Knudsen effect alone fails to describe
 354 our observations, and the major effect of significant decrease of the drying rate for the observed dry
 355 region thickness, becoming more important as the saturation decreases, has to be explained by other
 356 means.

357 Actually another effect may be at the origin of the deviation from our simple theory above. Let
 358 us first recall that this deviation occurs earlier, and thus at larger saturation, for decreasing particle
 359 diameter. Moreover, for smaller beads, namely, 6 and 12 nm diameter, no dry front at all can be
 360 observed, whereas the drying rate decreases to zero (see Fig. 2). This may be considered as being in
 361 the continuity of the effect observed at larger size: for very small bead size the slope in Fig. 3 would
 362 simply be vertical (i.e., constant h for increasing V). The original characteristics of drying for such
 363 small pores, i.e., an almost homogeneous desaturation with a significantly decreasing drying rate,
 364 suggests that our assumption concerning the vapor density value along the first wet interface is not
 365 valid here.

366 The origin of this feature is likely the Kelvin effect [39], which predicts that, if water vapor
 367 behaves as a perfect gas, in a medium in contact with a curved liquid-air interface the saturation
 368 vapor pressure is smaller than otherwise. The phenomenon finds its origin in the equality of the
 369 thermodynamic potential of the liquid, proportional to the pressure here equal to σ/r , where σ is
 370 the surface tension and r is the radius of curvature of the interface, with that of the gas, proportional
 371 to $\ln n_r$, where n_r is the relative humidity along a liquid-air interface. Under our experimental
 372 conditions this leads to $n_r = \exp -\frac{\sigma\Omega}{RT}(\frac{1}{r}) \approx \exp -0.54/r$, with Ω the water molar volume, R the
 373 gas constant, T the temperature in kelvins, and r expressed in nanometers. Note that the application
 374 of this calculation to a porous medium with complex and heterogeneous local liquid-gas interface
 375 shape is an approximation. From this estimation, we deduce that this effect becomes significant
 376 ($1 - n_r > 10\%$) for $r < 5$ nm. If we now simply assume again that evaporation mainly occurs
 377 around the most external liquid-air interface for nanoporous media which apparently remain wet
 378 up to the free surface (see Fig. 1), we get a drying rate equal to $V_r = n_r \rho_0 D_0 / \rho \delta$, which may be
 379 significantly lower than otherwise.

380 To compare this hypothesis to our results in a more accurate manner, we have to determine r as a
 381 function of the current (mean) saturation. We simply assume that, in the range of saturations [0.3–1]
 382 r varies like the thickness of the liquid films inside the sample, i.e., it is essentially proportional
 383 to R and ψ . Since we also know that it tends to infinity when $\psi \rightarrow 1$ and is of the order of the
 384 pore size (proportional to R) when $\psi \approx 0.5$, an expression which well reproduces all these trends
 385 is $r = \zeta R \psi / (1 - \psi)$. The factor ζ allows one to express the exact pore size value to be taken into
 386 account around the most external liquid-air interfaces, i.e., resulting from the saturation gradient at
 387 the approach of the free surface of the sample. Using this expression for r in the above drying rate
 388 equation we can compute the evolution of the relative drying rate (V_r / V_0) as the saturation decreases.
 389 Remarkably, with this model, we are able to reproduce very well the data for 6 and 12 nm with a
 390 single factor $\zeta = 1/4$ (see Fig. 2), which corresponds to a value for r close to a typical pore radius
 391 at $\psi \approx 0.5$, which seems in reasonable agreement with what we can expect when removing half the
 392 liquid volume from a bead packing. Note that this description assumes that for these nanoparticles
 393 most evaporation essentially occurs close to the top surface of the sample, which is certainly the
 394 case considering the almost homogeneous saturation profiles which imply that (even with the Kelvin
 395 effect) the vapor density gradient inside the medium will be very small. Finally our description
 396 assumes that capillary effects again play a major role. However, as we already remarked, when the
 397 liquid thickness is only a few times the molecule size, it remains unclear how with such effects one can
 398 still obtain a phenomenon of equilibration of the thickness of the liquid layer throughout the sample
 399 at any time during drying. Under such conditions our description through the Kelvin effect associated
 400 with reequilibrium may only be seen as a convenient simple approach in agreement with data.

DRYING REGIMES IN HOMOGENEOUS POROUS MEDIA . . .

401 Indeed, the Kelvin effect should *a priori* also take place during the drying of samples with larger
 402 pore sizes, since, as the saturation decreases, the liquid film thickness—and correspondingly the
 403 curvature radius of the menisci—decreases. According to the above estimations a significant impact
 404 of this effect should be observed for a saturation such that this radius of curvature is of the order
 405 of or below about 5 nm. Typically, with 40-nm bead diameter, the pore size is of the order of 6 nm
 406 (from geometrical estimations), so the radius of curvature of the menisci is of the same order at
 407 the beginning of drying. Thus, a significant decrease of drying rate as the saturation decreases is
 408 expected soon after the beginning of drying. For 80-nm beads a significant deviation can be expected
 409 below a saturation of the order of 40%, and for 300 nm, below about 10%. These estimations seem
 410 consistent with the starting points of deviation from the basic theory, observed in Fig. 2.

411 **C. Analysis of flow in the wet region**

412 Since we now have a clear view of the origin of the drying rate evolution as a function of the liquid
 413 distribution in time inside the sample it is interesting to see if we can predict this distribution and
 414 its evolution in time. Let us consider the receding front regime. Our data, providing rather precise
 415 information at low saturation, show that in contrast with some previous assumptions [4,17–19]
 416 this regime does not simply correspond to a growth of the apparent dry region. Indeed even when
 417 this region occupies a significant fraction of the sample the saturation in the wet region goes on
 418 decreasing almost homogeneously, more or less as in the CRP regime (but now with a significant
 419 saturation gradient at the approach of the dry region), and this is so down to extremely low saturation,
 420 approaching the minimal observable value [see Figs. 1(a)–1(f)]. For example, in Fig. 1(b) one may
 421 see that, for a saturation in the range 0.1–0.2, the dry front recedes significantly while the saturation
 422 decreases homogeneously over some significant sample thickness. In this context a critical question
 423 concerns the way the fluid is transported inside this wet region. Indeed we can consider two very
 424 different situations: a transport as liquid films through a connected network or a transport as vapor
 425 through the pores.

426 A transport as vapor is possible only if a significant gradient of saturation exists. As a matter of
 427 fact, such a gradient induces a gradient of liquid meniscus curvature, leading to a gradient of vapor
 428 density at equilibrium with the liquid (Kelvin effect). We write the spatial variation of saturation,
 429 $\Delta\psi$, and the corresponding variation of vapor density, Δn . Only then, a Fickian diffusion through
 430 the voids of the wet region (of thickness d) may occur. Let us estimate the drying rate associated
 431 with this process. It is equal to $V_g = \Delta n \rho_0 D'_v / \rho d$, in which $D'_v \approx (1 - \psi) D_v$. This transport is
 432 significant if the value of V_g is of the order of the drying rate of the sample, which was shown (see
 433 above) to be well estimated by considering vapor diffusion from the upper layers of the wet region,
 434 expressed as $V = n_r \rho_0 D_v / \rho (h + \delta^*)$. Thus, we have $V_g / V = (\Delta n / n_r) (1 - \psi) (h + \delta^*) / d$, which
 435 may also be written $V_g / V \approx (d \ln n) (1 - \psi) (h + \delta^*) / d$. Note that from the measured drying rate we
 436 know that δ^* is of the order of 1 mm. Assuming equilibrium and using again our above approximate
 437 expression for r we have $1/r \approx 4(1 - \psi) / R\psi$, so that we get $V_g / V \approx 2(1 - \psi) \Delta\psi (h + \delta^*) / R\psi^2 d$,
 438 in which R is expressed in nanometers. We can estimate this ratio from our data for the different
 439 bead sizes, by using values for the saturation, the thickness of the wet and dry regions, as they can be
 440 measured from Fig. 1. For bead diameters between 300 and 45 000 nm, the maximum value for the
 441 ratio $(h + \delta^*) / d$ is of the order of 5, and the maximum value for the saturation variation $\Delta\psi$ is of the
 442 order of 20% of ψ , so that in the domain where one can still observe an apparent plateau (in fact a
 443 region of slow spatial variations) of ψ in the wet region (typically for $\psi > 0.1$ except for the largest
 444 beads), we have. For the 80-nm beads, or for larger beads in the region of significant saturation
 445 gradient (either at the top of the wet region or in the very last stages of drying observed in our tests),
 446 we may find larger values for this ratio, typically of the order of 1, and the vapor transport through
 447 the wet region might be significant. Finally for smaller bead radii, in our range of observation, $\Delta\psi$
 448 is of the order of 0.1, ψ of the order of 0.5, and $h + \delta^* / d$ of the order of 1/5, so that V_g / V is much
 449 smaller than 1 and vapor transport in the wet region is negligible.

J. THIERY, S. RODTS, D. A. WEITZ, AND P. COUSSOT

450 We conclude that except for a narrow range of radii or in the ultimate stages of drying when
 451 water remains in the bottom layers of the sample, evaporation from inside the wet region and
 452 then transport towards the upper layers is negligible; however, by no means is the vapor transport
 453 significant in the homogeneously saturated regions. This implies that, to explain the desaturation of
 454 the wet region below the dry front, there must exist a continuous liquid network, made of liquid films
 455 possibly with liquid bridges at contact points, through which a significant transport process occurs.
 456 Under these conditions, here again, the homogeneous saturation decrease is associated with some
 457 capillary reequilibration processes. However, in contrast with the regime of initial homogeneous
 458 saturation decrease throughout the sample and associated with a constant drying rate, here the liquid
 459 transport velocity induced by the capillary effect is no longer sufficient to provide a liquid amount
 460 as large as that removed by evaporation. This explains that we now have at the same time an inward
 461 displacement of the dry front and a homogeneous desaturation in the wet region. Thus, the dry front
 462 progression results from some balance between evaporation and liquid flow in the wet region. In the
 463 following we focus on this liquid transport.

464 Thanks to our data providing a view of the liquid distribution in time we can get some information
 465 on the flow characteristics inside the wet region. More precisely we can compute the characteristic
 466 velocity of the liquid phase in this region. We focus on the liquid velocity through the upper section of
 467 the wet region. Since in the homogeneous saturation regions below the dry front the same approach
 468 based on mass conservation used for the CRP (see above) would show that the liquid velocity
 469 varies linearly with the distance, the velocity in each position is simply proportional to the velocity
 470 through the upper surface of the wet regions. In that aim we describe the liquid content in this region
 471 with the help of an average saturation ψ^* which, from the liquid mass conservation, is such that
 472 $H\bar{\psi} = (H - h)\psi^*$. Deriving this equation we deduce the expression for the mean velocity of the
 473 liquid phase per unit surface, $V_L = -\varepsilon(H - h)(d\psi^*/dt) = V - \varepsilon\psi^*(dh/dt)$, which is represented
 474 in the inset of Fig. 2. Considering the gradient of saturation extending over a significant sample
 475 thickness in the FRP regime it is tempting to assume that the liquid flow can simply be described by
 476 Darcy's law for a partially saturated flow through a porous medium under the effect of a pressure
 477 gradient. This gives a velocity $V_L = -(k/\mu)\nabla p$, where ∇p is the pressure gradient, μ the liquid
 478 viscosity, and k the permeability of the liquid network (unsaturated porous medium). The typical
 479 pressure is the Laplace pressure $p = \sigma/r(\psi^*)$, where $r(\psi^*)$ is the mean radius of curvature of the
 480 liquid-air interface in the region of saturation ψ^* . $r(\psi^*)$ scales with the bead radius and it may
 481 be shown from basic geometrical considerations that at low saturation the radius of curvature of
 482 the interface around the points of contact between the grains is proportional to $\sqrt{\psi^*}$. The typical
 483 length scale for the extent of pressure variation is the sample thickness H . On the other hand, we
 484 know that the permeability k scales with the square of the mean liquid channel thickness (e) via a
 485 constant factor of the structure, for example equal to $1/8$ for straight parallel ducts. e is equal to
 486 the ratio of the liquid volume per bead, i.e., $4(\varepsilon/1 - \varepsilon)\pi R^3\psi^*/3$, and to the corresponding solid
 487 area, i.e., $4\pi R^2$, which gives $e = uR\psi^*$ with $u = \varepsilon/1 - \varepsilon$ (ε being the porosity), so that we write
 488 $k = \beta R^2\psi^{*2}$, where β is a characteristic of the porous structure. We finally get

$$V_L \propto (\sigma/\mu H)\psi^{*1.5}R. \quad (2)$$

489 Our data show an approximate scaling of the type $V_L \propto (\psi^*/\psi_c)^{1.5}$ in agreement with this
 490 expression (see inset of Fig. 3) concerning the variation with ψ^* . However, here the dependence
 491 on R is only expressed through the variation with ψ_c . Indeed, in the representation of the inset
 492 of Fig. 3 the data for $V_L(\psi^*/\psi_c)$ are situated in a narrow area without any apparent monotonous
 493 variation of their level with R . Since $\psi_c \propto R^{-1/4}$ (see inset of Fig. 2) we thus deduce essentially
 494 $V_L(R) \propto \psi_c^{-1.5} \propto R^{0.37}$. This means that the expected scaling as R of Eq. (2) does not apply at all
 495 over our four-decade range of pore sizes. This suggests that the "classical hydrodynamic description"
 496 assumed above is not appropriate in this context.

497 Actually, this result might be due to the specific process of capillary reequilibration in the CRP,
 498 assumed to be similar in the FRP in the wet regions where the saturation remains homogeneous. As

DRYING REGIMES IN HOMOGENEOUS POROUS MEDIA . . .

499 already mentioned this process relies on successive steps of redistribution of saturation throughout
 500 the medium, allowing the Laplace pressure to be uniform at any time between two such events. So it
 501 does not seem clear that this process is equivalent to a flow on average governed by a simple gradient
 502 of Laplace pressure along the main flow direction through an (almost) constant liquid network.
 503 Instead, there might be strong variations of the local Laplace pressure between two successive
 504 reequilibration events throughout the medium. These variations of the driving force could finally
 505 induce some different average hydrodynamic behavior of the system.

IV. CONCLUSION

506
 507 NMR provides a robust approach to the study of confined liquid flow down to the molecular
 508 scale by averaging over a macroscopic sample. Investigating drying on a variety of model porous
 509 media through dynamic MRI measurements provided us with saturation profiles in time down to
 510 molecular liquid film and close to complete evaporation for a wide range of pore sizes. Consistent
 511 with what was so far essentially shown for packings of relatively large beads, a CRP associated with
 512 homogeneous desaturation is shown to exist down to bead sizes of a few hundred nanometers. A
 513 falling rate period then occurs as an apparent dry region develops. During that stage, we verified
 514 the variations in the drying rate being governed by the diffusion of vapor through the apparent dry
 515 zone. For small pore sizes one could expect the impact of the Knudsen effect, inducing a decrease
 516 of the diffusion coefficient when the pore size decreases, due to the increasing collision rate of
 517 gas molecules to the matrix walls. However, such an effect was not clearly observed in our tests.
 518 Finally, the drying rate proved essentially to be increasingly reduced because of the effect of interface
 519 curvature, i.e., the Kelvin effect. In particular, we demonstrated that the former effect fully governs
 520 the kinetics of drying in nanoporous media for which, surprisingly, a homogeneous desaturation is
 521 observed whereas standard capillary effects can hardly play a major role in this situation.

522 This study especially reveals that the saturation decreases approximately homogeneously
 523 throughout the wet regions of the material even if a dry front develops. This proves the existence
 524 of a continuous liquid network capable of draining towards the interface of higher evaporation all
 525 along drying and whatever the pore size. This phenomenon results from capillary reequilibration
 526 effects as in the CRP. In this framework, we proved that the scaling with the pore size expected when
 527 assuming that the liquid is transported upwards through its own network driven by a standard value
 528 of the Laplace pressure does not correspond to our data.

529 Our results show that the flow of liquid in drying porous media exhibits original trends, and
 530 complex effects start to play a role for very small pores, which need to be further studied. This might
 531 in particular provide complementary information to the usual studies concerning the properties of thin
 532 liquid films (at a scale of the order of the nanometer). We also showed that capillary reequilibration
 533 effects play a major role at any time during drying, even at extremely low saturation, i.e., with
 534 thin liquid films. This phenomenon is poorly known and should be further studied to reach a full
 535 description of the processes occurring during drying: in particular, the transition from the CRP to
 536 the FRP and during the FRP.

-
- [1] J. Van Brakel, Mass transfer in convective drying, *Adv. Drying* **1**, 217 (1980).
 [2] J. B. Laurindo and M. Prat, Numerical and experimental network study of evaporation in capillary porous media, *Chem. Eng. Sci.* **53**, 2257 (1998).
 [3] I. N. Tsimpanogiannis, Y. C. Yortsos, S. Poulou, N. Kanellopoulos, and A. K. Stubos, Scaling theory of drying in porous media, *Phys. Rev. E* **59**, 4353 (1999).
 [4] P. Coussot, Scaling approach of the convective drying of a porous medium, *Eur. Phys. J. B* **15**, 557 (2000).
 [5] F. Chauvet, P. Duru, S. Geoffroy, and M. Prat, Three Periods of Drying of a Single Square Capillary Tube, *Phys. Rev. Lett.* **103**, 1 (2009).

J. THIERY, S. RODTS, D. A. WEITZ, AND P. COUSSOT

- [6] D. Or, P. Lehmann, E. Shahraeeni, and N. Shokri, Advances in soil evaporation physics—A review, *Vadose Zone J.* **12** (2013).
- [7] N. Prime, Z. Housni, L. Fraikin, A. Leonard, R. Charlier, and S. Levasseur, On water transfer and hydraulic connection layer during the convective drying of rigid porous material, *Transp. Porous Media* **106**, 47 (2015).
- [8] P. Coussot, C. Gauthier, D. Nadji, J. C. Borgotti, P. Vié, and F. Bertrand, Capillary motion during drying of a granular paste, *C.R. Acad. Sci., Paris* **327**, 1101 (1999).
- [9] L. Pel, H. Brocken, and K. Kopinga, Determination of moisture diffusivity in porous media using moisture concentration profiles, *Int. J. Heat Mass Transfer* **39**, 1273 (1996).
- [10] P. Faure and P. Coussot, Drying of a model soil, *Phys. Rev. E* **82**, 036303 (2010).
- [11] G. H. A. van der Heijden, L. Pel, H. P. Huinink, and K. Kopinga, Moisture transport and dehydration in heated gypsum, an NMR study, *Chem. Eng. Sci.* **66**, 4241 (2011).
- [12] A. Yiotis, D. Salin, E. Tajer, and Y. Yortsos, Drying in porous media with gravity-stabilized fronts: Experimental results, *Phys. Rev. E* **86**, 026310 (2012).
- [13] P. Lehmann, S. Assouline, and D. Or, Characteristic lengths affecting evaporative drying of porous media, *Phys. Rev. E* **77**, 056309 (2008).
- [14] N. Shokri, P. Lehmann, P. Vontobel, and D. Or, Drying front and water content dynamics during evaporation from sand delineated by neutron radiography, *Water Resour. Res.* **44**, 06418 (2008).
- [15] N. Shokri and D. Or, What determines drying rates at the onset of diffusion controlled stage-2 evaporation from porous media? *Water Resour. Res.* **47**, W09513 (2011).
- [16] N. Grapsas and N. Shokri, Acoustic characteristics of fluid interface displacement in drying porous media, *Int. J. Multiphase Flow* **62**, 30 (2014).
- [17] N. Ceaglske and O. A. Hougen, Drying granular solids, *Trans. Am. Inst. Chem. Eng.* **33**, 283 (1937).
- [18] S. Whitaker and W. T. H. Chou, Drying granular porous media-theory and experiment, *Drying Technol.* **1**, 3 (1983).
- [19] P. Chen and D. C. T. Pei, A mathematical model of drying processes, *Int. J. Heat Mass Transfer* **32**, 297 (1989).
- [20] N. Shahidzadeh-Bonn, A. Azouni, and P. Coussot, Effect of wetting properties on the kinetics of drying of porous media, *J. Phys.: Condens. Matter* **19**, 112101 (2007).
- [21] M. D. Seck, E. Keita, P. Faure, P. Cavalié, M. Van Landeghem, S. Rodts, and P. Coussot, Subflorescence and plaster drying dynamics, *Chem. Eng. Sci.* **148**, 203 (2016).
- [22] E. Keita, P. Faure, S. Rodts, and P. Coussot, MRI evidence for a receding-front effect in drying porous media, *Phys. Rev. E* **87**, 062303 (2013).
- [23] E. Keita, T. E. Kodger, P. Faure, S. Rodts, D. A. Weitz, and P. Coussot, Water retention against drying with soft-particle suspensions in porous media, *Phys. Rev. E* **39**, 23 (2016).
- [24] J. Thiery, E. Keita, S. Rodts, D. Courtier Murias, T. Kodger, A. Pegoraro, and P. Coussot, Drying kinetics of deformable and cracking nano-porous gels, *Eur. Phys. J. E* **39**, 117 (2016).
- [25] J. Thiery, S. Rodts, E. Keita, X. Chateau, P. Faure, D. Courtier-Murias, T. E. Kodger, and P. Coussot, Water transfer and crack regimes in nanocolloidal gels, *Phys. Rev. E* **91**, 042407 (2015).
- [26] G. C. Kuczynski, Study of the sintering of glass, *J. Appl. Phys.* **20**, 1160 (1949).
- [27] D. A. Weitz and M. Oliveria, Fractal Structures Formed by Kinetic Aggregation of Aqueous Gold Colloids, *Phys. Rev. Lett.* **52**, 1433 (1984).
- [28] *Signal Treatment and Signal Analysis in NMR*, edited by D. N. Rutledge (Elsevier Science, New York, 1996), Vol. 18.
- [29] P. T. Callaghan, *Principles of Nuclear Magnetic Resonance Microscopy* (Clarendon, Oxford, UK, 1993).
- [30] T. M. Shaw, Drying as an Immiscible Displacement Process with Fluid Counterflow, *Phys. Rev. Lett.* **59**, 1671 (1987).
- [31] A. G. Yiotis, A. G. Boudouvis, A. K. Stubos, I. N. Tsimpanogiannis, and Y. C. Yortsos, Effect of liquid films on the drying of porous media, *AIChE J.* **50**, 2721 (2004).
- [32] L. Xu, S. Davies, A. B. Schofield, and D. A. Weitz, Dynamics of Drying in 3D Porous Media, *Phys. Rev. Lett.* **101**, 094502 (2008).

DRYING REGIMES IN HOMOGENEOUS POROUS MEDIA . . .

- [33] J. Thiery, Water transfers in sub-micron porous media during drying and imbibition, Ph.D. thesis, Université Paris-Est, 2016.
- [34] A. A. Moghaddam, A. Kharaghani, E. Tsotas, and M. Prat, Kinematics in a slowly drying porous medium: Reconciliation of pore network simulations and continuum modeling, *Phys. Fluids* **29**, 022102 (2017). 6
- [35] E. Keita, S. A. Koehler, P. Faure, D. A. Weitz, and P. Coussot, Drying kinetics driven by the shape of the air/water interface in a capillary channel, *Eur. Phys. J. E* **39**, 23 (2016).
- [36] M. Suzuki and S. Maeda, On the mechanism of drying of granular beds, *J. Chem. Eng. Jpn.* **1**, 26 (1968).
- [37] P. Lehmann and D. Or, Effect of wetness patchiness on evaporation dynamics from drying porous surfaces, *Water Resour. Res.* **49**, 8250 (2013).
- [38] B. Coasne, A. Galarneau, R. J. M. Pellenq, and F. Di Renzo, Adsorption, intrusion and freezing in porous silica: The view from the nanoscale, *Chem. Soc. Rev.* **42**, 4141 (2013).
- [39] J. F. Daian, *Equilibrium and Transfers in Porous Media* (Wiley, New York, 2014).